X-Ray Inspection Model Validation with Physical Dosimetry

Michael P. Pfeifer[1,2*], Nathanael Simerl[1], John Porter[2], Dr Walter J. McNeil[1] and Dr Amir A. Bahadori[1]

[1*]Alan Levin Department of Mechanical and Nuclear Engineering, Kansas State University, Ward Hall, 1200 N M.L.K. Jr. Dr, Manhattan, 66506, KS, USA.
[2]Honeywell Federal Manufacturing & Technologies, 14510 Botts Rd, Kansas City, 10587, MO, USA.

*Corresponding author(s). E-mail(s): MPfeifer@kcnsc.doe.gov;

Abstract

A non-functional printed circuit board assembly (PCBA) was developed using ULTIboard and a simple computational transport model was created for use with the Monte Carlo software MCNP. EBT3 film radiography was used to compare with Monte Carlo simulation to validate the board representation. The [c1]computational transport model was then revised to include connection pins, solder balls, highly attenuating internal structures, and copper trace distribution. Results from the secondary model were compared to the EBT3 films to observe improvements to dose profiles. It was found that this method was useful in verifying the placement of components as the dose profiles were observed to follow the same trends. The experiment was then repeated using XRQA2 films to achieve the same level of contrast with [c2]1% the dose of EBT3 films. It was found that high contrast may be achieved through these films to identify major issues with the model geometry, at a cost of accuracy to the magnitude of the dose profiles. A second

This work was funded by the Department of Energy's Kansas City National Security Campus, operated by Honeywell Federal Manufacturing & Technologies, LLC under contract number DE-NA0002839.

[c1] *MPP*: *Text added.*
[c2] *MPP*: ~~100 times less dose than that of~~

validation method was applied to the model using 37 CaF_2 thermoluminescent dosimeters (TLDs). TLD measurements were compared with the simplified and complex transport models to observe what features have the largest impact to simulation accuracy. The TLD calibration to CaF_2 was found to be accurate within 5.6%, while calibration to a dose in Si was found to be accurate within 4.7%. It was observed that the largest impact on TLD dose was [c3]accurate representation of solder balls, and proper modeling of highly attenuating internal structures.

Keywords: Ball grid array, X-ray system, Radiography, Monte Carlo, Electronics Inspection

1 Introduction

Ball grid arrays (BGAs) are surface-mount packages that are increasingly being used to replace pin grid arrays (PGAs) in high-speed electronics due to superior properties in connection density, heat conduction, and impedance [1]. Unlike PGAs, which use a mechanical socket connection, BGAs are soldered directly to the printed circuit board (PCB), which reduces the system size and weight. While these devices offer improved performance, they are permanently connected to the PCB and must be thoroughly inspected via X-ray imaging to ensure that the BGA is free of connection defects such as incorrect solder placement, inadequate re-flow, and solder ball voiding [2]. During the inspection process, board components are exposed to ionizing radiation, which over time can damage semi-conductor components and result in failure of the PCB assembly (PCBA). To minimize the risk of radiation effects, dose limits are typically set for individual components based on their electronic function, composition, and relative importance to operation. For electronics, these dose limits are often expressed as dose in silicon (Si) [3][4]. However, many components contain high atomic number materials and have high density, which puts these components at risk of exceeding dose limits [5]. Currently, Monte Carlo simulation is the most practical method to provide absorbed dose estimates for PCBA components. However, Monte Carlo models are often simplified[c1] to save time and computational resources. The concern is that model accuracy may suffer due to oversimplification. Therefore, a validation of the model must be performed using direct measurements.

The purpose of this study was to use film measurement to validate the source positioning and part placement within [c2]the computational transport model and to use TLDs to compare measured dose results with estimated results to validate attenuation properties. To do this, a non-functional PCBA was designed and fabricated to provide computational and physical models.

[c3] *MPP*: ~~attributed to solder balls representation~~

[c1] *MPP*: ~~in order~~

[c2] *MPP*: *Text added.*

The initial computational model [c3]was designed to be a simplified [c4]representation directly converted from the PCBA design software ULTIboard 2019 [6]. EBT3 film radiography measurements were [c5]then used to determine necessary model improvements [7]. These results [c6]of EBT3 measurements were [c7]then implemented to develop a complex [c8]transport model to better characterize the PCBA. Dose calibration was then performed on the EBT3 film to compare attenuating properties between the computational and experimental models. By comparing the dose profiles of the measured film to the dose profiles produced through Monte Carlo simulation, model accuracy was characterized. This was repeated using XRQA2 films to determine whether the same analysis can be completed using dose rates achievable in a fluoroscopic X-ray system [8]. [c9]Thermoluminescent dosimeter (TLD) measurement and simulation techniques were then [c10]applied to obtain dose rate estimates. [c11]The TLDs were placed in areas of high importance or areas of questionable representation [c12]to gauge model accuracy. Since PCBA components are typically given dose limits in terms of absorbed dose in Si, a study was performed on calibrating CaF_2 TLDs to Si dose while maintaining accuracy.

2 Materials and Methods

2.1 Development of Test PCBA

To simulate the design process of creating a printed circuit board, a non-functional PCBA was developed by the Kansas State University Electronics Design Laboratory (KSU-EDL). To keep the design true to boards of interest, the board was populated with over 900 parts, used 20 different types of components, and contained two BGAs and 10 copper layers. Five copies of the board were manufactured for film and TLD experimentation. The [c1]PCBA design was exported from ULTIboard as a *.step file to be further edited into a Monte Carlo ready model. [c2]Along with the 3D model, the copper traces of each layer of the PCB were exported as *.xml files. Parts used on the board, their manufacturer, their quantity, and a brief description are given in Table 1.

2.2 Simplified Transport Model

In Monte Carlo simulation, geometries are usually represented using second-order surfaces. The challenge is determining the appropriate level of detail to

---

[c3] *MPP*: ~~was a~~
[c4] *MPP*: ~~model~~
[c5] *MPP*: *Text added.*
[c6] *MPP*: *Text added.*
[c7] ~~used~~
[c8] *MPP*: *Text added.*
[c9] *MPP*: ~~Themoluminescent~~
[c10] ~~used~~
[c11] ~~These~~
[c12] *MPP*: *Text added.*
[c1] *MPP*: *Text added.*
[c2] *MPP*: ~~With~~

Distributor	#	Part ID	Volume (mm^3)	Density ($g\,cm^{-3}$)	Description
Digi-key	16	AVX Corporation TAJD226K020SNJ	97.309	3.22	22 uF Molded Tantalum Capacitor
TME (Poland)	348	Samsung Electro-Mechanics CL10C102JB8NNND	1.152	5.14	1000 pF Ceramic Capacitor
Newark (UK)	310	Yageo RC0603FR-0710KL	0.704	0.87	10 kOhm Resistor
Newark (UK)	32	Kemet C0402C101J3GACTU	0.275	4.40	100 pF Ceramic Capacitor
Digi-key	8	STMicroelectronics M74HC368RM13TR	70.000	3.40	IC Buffer Invert 6V
Digi-key	124	Microchip Technology MCP6241-E/SN	33.442	2.11	IC Op Amplifier
Newark (UK)	4	Microchip Technology MIC5504-3.3YM5-TR	6.728	1.23	IC REG LINEAR 3.3V 300mA
Digi-key	6	TXC CORPORATION 7W-12.000MBA-T	45.500	3.36	12 MHz CMOS Oscillator 3.3V
Digi-key	8	Rohm Semiconductor TCM0J106M8R	1.088	5.51	10 uF Tantalum Capacitor
Digi-key	2	Lattice MDS FG484 LCMXO2-4000HC-4FG484C	1058.000	3.03	Field Programmable Gate Array
Digi-key	6	Vishay Sprague 293D106X0016C2TE3	48.000	2.19	10 uf Tantalum Capacitor
Digi-key	20	Nexperia 74HC4053PW,112	21.802	2.92	Single-ended Multiplexer
Digi-key	8	Samsung Electro-Mechanics CL31C750JBCNNNC	5.120	5.94	75 pF Ceramic Capacitor
Digi-key	8	Diodes Incorporated PAM2320BECADJR	26.163	3.08	Switching Voltage Regulator
Future	6	On Semi NCP5501DT50RKG	99.628	3.37	Low Dropout Linear Voltage Regulator
Digi-key	16	Yageo RC0402FR-071KL	0.175	3.40	1 kOhm Resistor
Digi-key	6	Microchip Technology ATSAM3N0BA-AU	68.6	2.49	ARM Micro-controller
Digi-key	30	On Shore Technology Inc. 302-S101	762.694	1.90	Connector Header
Digi-key	2	Laird-Signal Integrity Products HZ0603B102R-10	1.216	4.76	1 kOhm Ferrite Bead

Table 1: Distributor, quantity, part name, volume, density, and part description for all components on test PCBA.

accurately model the PCBA while keeping the model simple enough for manageable run times and data extraction. If the PCBA model is too complex, leads, traces, and internal structures could lead to overlapping geometries, which will result in the failure of the unstructured mesh. If the geometry is overly simplified, inaccurate dose estimates could result. As a starting point, the level of detail in the CAD geometry was kept to a minimum. The CAD model was exported from ULTIBoard and imported into SolidWorks 2020 [9] for editing. Unfortunately, it was found that direct import between these two software packages led to hundreds of broken geometry errors. To fix this issue, the CAD translation software TransMagic was used [10]. This program intelligently attempts to create a water-tight geometry by correcting overlapping surfaces, removing flawed surfaces, and replacing [c3]the surfaces of open geometries with a series of geometric planes. [c4]Individual planes are then 'knitted' into [c5]solid bodies resulting in a corrected volume.

[c1]The geometry exported from ULTIboard was found to represent surfaces and volumes by extruding component silkscreens. The corrected components from TransMagic were found to have accurate placement but incorrect dimensions. Manual edits were made to the CAD geometry [c2]to correct part sizing based on manufacturer data and caliper measurement. Parts with complex shapes, such as connection headers and programmable gate arrays, were redesigned based on manufacturer dimensions. To avoid meshing issues that can arise from node sharing between [c3]components and the board, [c4]all parts were offset to float 1 µm from the board surface. The finished model properly represented all the components on the board as simple structures, and modeled the PCB as one homogeneous volume. SolidWorks renderings of the PCBA for the simple representation are given in Figure 1.

[c3] *MPP*: ~~flaws~~
[c4] *MPP*: ~~The individual~~
[c5] ~~volumes~~
[c1] *MPP*: ~~Since ULTIboard builds surfaces based on silkscreens, the parts after the TransMagic corrections had the correct placement but incorrect dimensions.~~
[c2] *MPP*: ~~using~~
[c3] *MPP*: ~~the parts~~
[c4] *MPP*: ~~the~~

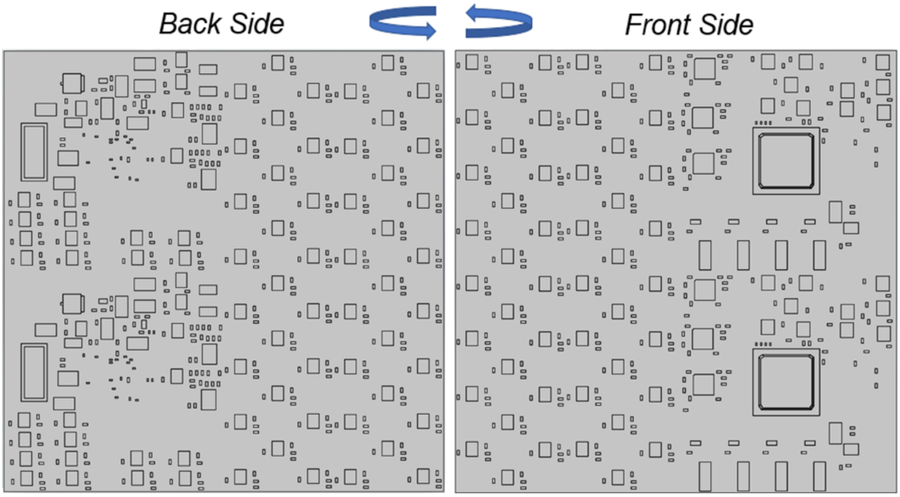

Fig. 1: SolidWorks model for simplified geometry.

2.3 Initial Film Comparison

The simple CAD model represented the component volume and placement but lacked features such as board layers, [c5]the solder ball representation of the BGAs, and pin-outs for the connection headers. To determine the spacing of the BGAs, and the importance of the PCB traces, [c6]measurements using radiochromic EBT3 film were performed. These films are created and distributed by Ashland, are self-developing, and have an effective dose range of 0.1-10 Gy [7]. An irradiation was performed with a Rad Source RS1800 X-ray generator [11]. To keep this device consistent with exposure settings used during BGA inspection, an expert was contacted about standard operating procedures. Typical operation for this board type was determined to be at a tube voltage of 130 kV and a power of 10 W[c7]. A 0.0254 cm zinc filter was used to reduce low energy X-rays, and a 0.127 cm aluminum filter was used to simulate attenuation through a sample tray. [c8] [c9]For the test PCBA irradiation, the film was secured to the bottom tray (Shelf1), 37.1 cm from the source. Plastic standoffs were used to level the PCBA 1 cm above the film. The suggested tube voltage of 130 kV and maximum tube current of 10 mA was used for a 10 min irradiation.[c10] [c11]The film was scanned at 75 dpi and converted to grayscale to provide a high-contrast image. Because this stood as an initial comparison to determine discrepancies within the simplified model geometry,

---

[c5] *MPP*: ~~solder balls on the underside~~
[c6] *MPP*: ~~radiography with EBT3 film was performed~~
[c7] *MPP*: ~~to obtain optimal contrast~~
[c8] *MPP*: ~~For the test PCBA irradiation, the tube voltage was set to 130 kV, and the tube potential was set to 10 mA.~~
[c9] *MPP*: *Text added.*
[c10] ~~A 0.0254 cm zinc and 0.127 cm aluminum filter were used and the irradiation time was 10 min.~~
[c11] *MPP*: ~~After the irradiation, the~~

a film calibration procedure was not needed. The EBT3 grayscaled image and labeled areas of interest are shown in Figure 2.

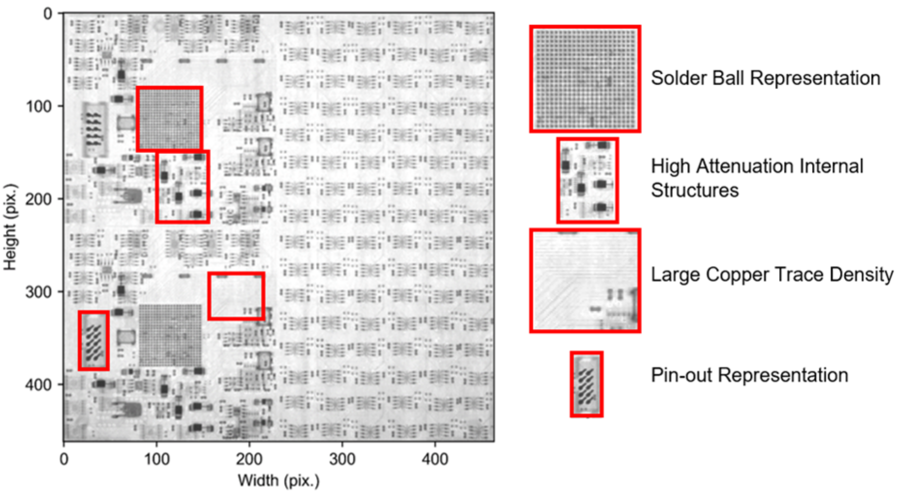

Fig. 2: EBT3 film irradiation to determine problematic areas with simplified PCBA model.

2.4 Complex Transport Model

From the initial test irradiation, it was found that significant improvements to the Monte Carlo model were feasible. The first major feature to be improved was the representation of the solder ball array. This feature is particularly important, as the LCMX02 processor is the largest, most sensitive, and most important item on the PCBA. To represent the solder ball array, a single solder ball was assembled into a 22×22 array using the linear component pattern feature in SolidWorks. A sub-study was performed using the radiography tally feature within the Monte Carlo N-Particle (MCNP) [12] code to check if the representation of the solder ball array was accurate. After testing spheres, icosahedrons, dodecahedrons, and extruded decagons, it was found that the most accurate simulated radiography images were produced using the extruded decagon shape[c1]. The radius of each decagon was calculated from a pixel count in the initial film measurement. The extrusion height, was chosen to conserve the total volume and mass an individual solder ball. The [c2]solder ball representation was added to the model on the underside of the LCMX02 processors. [c3]The implementation of the solder ball arrays for the LCMX02 BGAs is shown in Figure 3.

[c1] ~~, conserving the total volume in an individual solder ball~~
[c2] ~~extruded decagon array~~
[c3] *MPP*: ~~An example of the~~

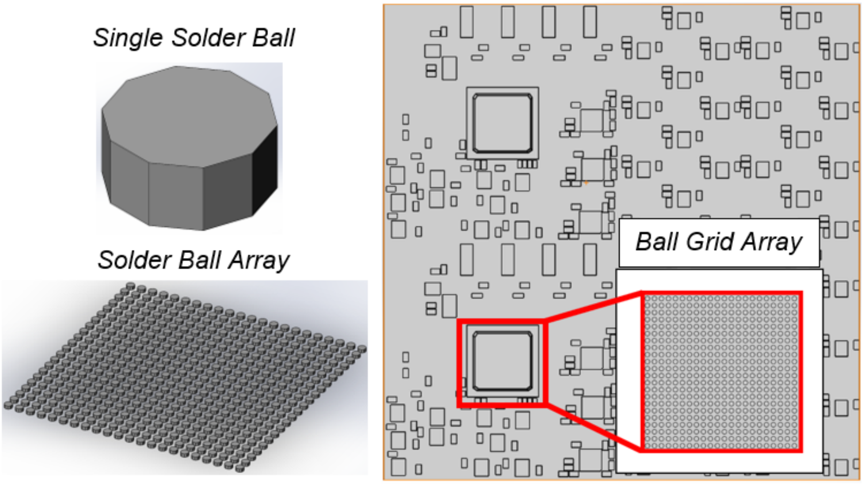

Fig. 3: Example of BGA representation in CAD model geometry using SolidWorks and linear component pattern.

The copper representation throughout the board was achieved through a voxelization method due to complexities associated with direct representation. The individual voxel sizes were 3 mm×3 mm×1.5 mm and were combined into a 50×50 grid of voxels to represent the PCB. This permitted [c4]discrete material assignments to each voxel based on copper concentration. [c5]The copper concentration of each voxel was determined using *.pdf images of the board layers. [c6]These images were converted to grayscale, and the number of dark pixels (copper) to the number of white pixels (void) were used to calculate the ratio of copper to glass fiber material. Representative images are shown in Figure 4. It can be seen that the signal layers are generally devoid of copper traces except for around the BGA region, while the power layers have high concentrations of copper everywhere except for the BGA locations. When combined, this shows clearly that the BGA region is largely devoid of copper concentration with the run-off traces from the BGA having significantly higher copper concentration.

The last two features included were the pin-out representation and the high-attenuating structures. The pin-out representation was achieved by measuring the length and width of the pins, inserting them in the model, and subtracting the intersecting volumes. While this change is not expected to have a large impact on simulation results, the material definitions for the connection headers changed substantially, as the copper and zinc connections made up a large portion of the total mass[c1]. Separating this sub-component drastically changes the density representation of the plastic connection [c2]as it no longer accounts

[c4] ~~individual material assignment for~~
[c5] *MPP*: ~~To determine the copper concentration of each voxel, *.pdf images of each layer~~
[c6] *MPP*: *Text added.*
[c1] *MPP*: ~~for the component~~
[c2] *MPP*: ~~features as they no longer compensate for the pin mass~~

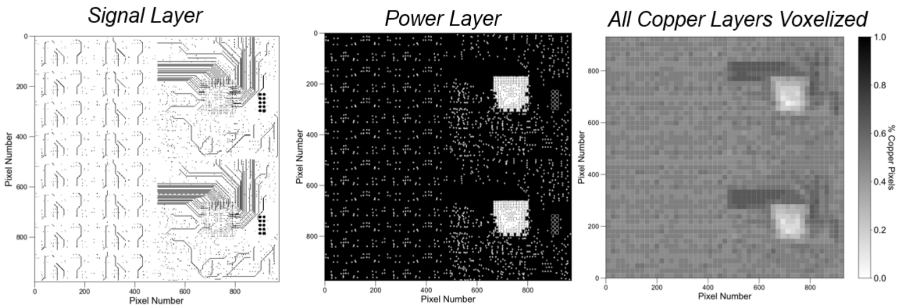

Fig. 4: Example of board voxelization to represent copper distribution through PCBA.

for the pin mass. [c3]The initial film measurement showed two types of capacitors to contain highly attenuating internal structures composed of tantalum oxide and manganese-II layers. Tantalum oxide has a density of 8.2 g cm^{-3} and accounts for approximately 46% of the part's total mass. Considering capacitor size, homogenizing the tantalum throughout the entire part (as in the simplified model) results in a larger [c4]attenuated region, which can greatly impact the dose to surrounding parts. To represent these parts, the pixels from the scanned film were counted to obtain estimates for the length and width of the tantalum block. The block was then extruded, conserving the mass of tantalum included in the part. When producing a mesh [c5]for MCNP, components can not be encapsulated [c6]within another component [13]. To resolve this issue, a small cap is introduced [c7]to encase the tantalum block between two surrounding volumes. An example of tantalum capacitor representation is given in Figure 5. Images of the finalized CAD model for the test PCBA are given in Figure 6.

2.5 Simulated Source Term

For all irradiations [c1]and measurements, the Rad Source RS1800 X-ray generator was used. This device [c2]is capable of tube voltage ranging from 40 to 160 kV and tube current ranging between 1 to 10 mA. A 0.0254 cm zinc filter and a 0.127 cm aluminum filter were used to represent common filtration and the irradiation tray used during BGA inspection. [c3]Visualization of the BGAs on a commercial system showed a tube voltage of 130 kV gave optimal contrast during inspection. To simulate [c4c5]this spectrum, the program SpekCalc

[c3] *MPP*: ~~Two types of capacitors were found to~~
[c4] ~~attenuation~~
[c5] *MPP*: ~~in~~
[c6] *MPP*: ~~in~~
[c7] *MPP*: ~~to act as if the tantalum block is encased~~
[c1] *MPP*: *Text added.*
[c2] *MPP*: ~~applies a tube voltage of 130 kV and power~~
[c3] *MPP*: *Text added.*
[c4] *MPP*: ~~the source spectra~~
[c5] *MPP*: *Text added.*

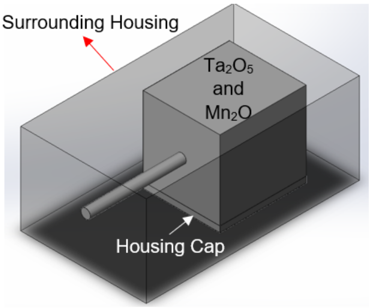

Fig. 5: Representation of tantalum oxide and manganese-II attenuating structure in complex CAD model.

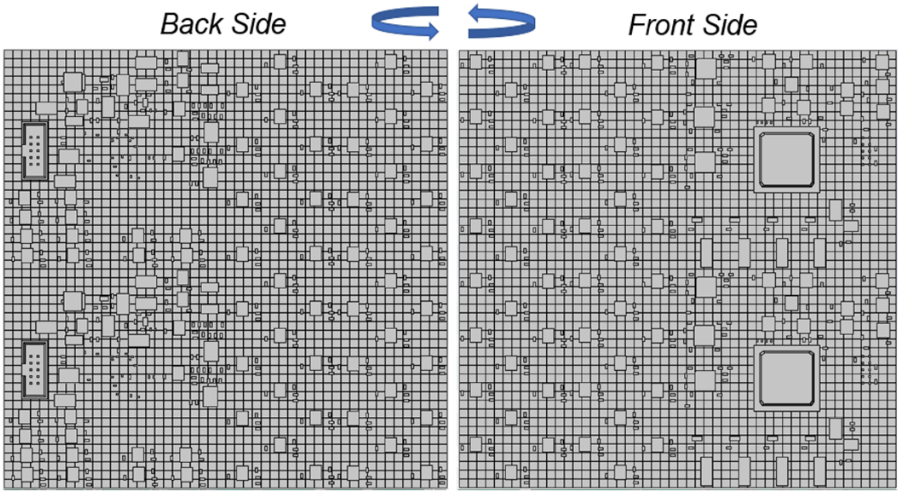

Fig. 6: SolidWorks model for fully detailed geometry used with MCNP.

was used to provide [c6]the estimated X-ray beam output [c7] [c8]for a tungsten anode at a 30° anode angle [14]. [c9]The spectrum generated by SpekCalc is passed to MCNP as a probability density function (PDF). The random number generator of MCNP samples the PDF to determine the particle energy. The program will then sample the particle direction, path length, and interaction type based on the material properties present. The MCNP output is a readable text file containing the radiation dose of each cell in a per-source particle format. This result is scaled in post-processing using the machine source strength, the irradiation time, and a solid angle correction factor. The source strength and location of the Rad Source RS1800 were found by comparing ion chamber

[c6] *MPP*: ~~a~~
[c7] ~~for a tungsten anode operating at 130 kV. The anode angle was set to with a 30° anode angle~~
[c8] *MPP*: *Text added.*
[c9] *MPP*: *Text added.*

measurements with simulated results. [c10]Ion chamber measurement estimated the X-ray source strength to be ≈1.35×10^{14} photons per second. Intensity measurements on each shelf estimated the source location at ≈37.1 cm above the bottom shelf (Shelf1). A simplified MCNP model including the source, the filtration, and the irradiation tray, confirmed that the simulated dose is within 5% error up to 10 cm from the center of Shelf1 [15]. The X-ray beam output estimated by SpekCalc and the shelf dose profile produced through ion chamber simulation and measurement are shown in Figure 7.

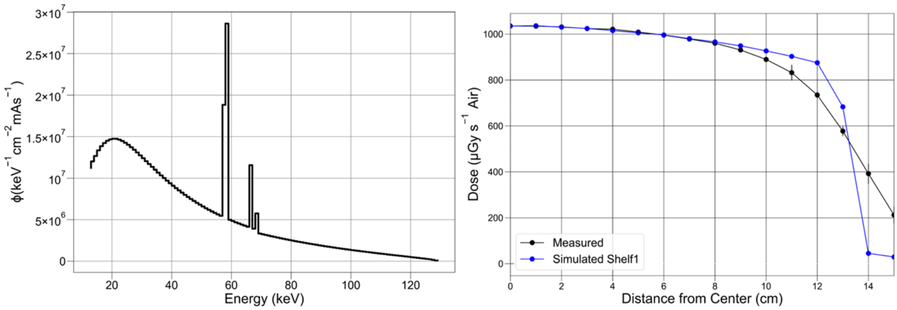

Fig. 7: Example of 130 kV source spectra (left) and measured vs. simulated dose profile accuracy (right) for RS1800 X-ray generator.

2.6 Film Radiography

Material properties for all [c1]PCBA components were obtained from manufacturers or distributors. Due to proprietary or missing materials, seven of the 20 components had errors introduced to their composition. Of the parts with missing materials, five had errors less than 1% while two components had errors between 1 and 3.2% of the total mass. [c2]To validate the material assignments for the Monte Carlo model, Gafchromic EBT3 films were used. [c3] [c4]When exposed to ionizing radiation, EBT3 film will exhibit a change in color from green to blue. The intensity and depth of the color change is proportional to the radiation dose received. To express the radiation dose, a set of calibration films must be generated by exposing the films to a range of known doses (in tissue). After irradiation, these films will continue to undergo polymerization with time. Therefore, a 24-hour development period was established between

[c10] *MPP*: ~~Using an ion chamber, the X-ray source location was estimated to be 37.1 cm above the bottom shelf (Shelf1).~~

[c1] *MPP*: ~~parts~~

[c2] *MPP*: ~~As validation for~~

[c3] *MPP*: ~~To obtain dose estimates, a set of calibration films must be applied to properly scale scanned pixel values. This calibration set was created by exposing the EBT3 films to a range of known doses (in tissue) and then scanning the films using a photo scanner with a transparency unit. Each irradiated region was then sampled and disassembled into its average red, green, and blue (RGB) intensity values.~~

[c4] *MPP*: *Text added.*

the irradiation and photo scan for all film measurements. Calibration films were exposed to the 130 kV beam of the Rad Source RS1800. Irradiation times for each exposure were adjusted to give a known dose based on ion chamber measurement. After the 24-hour development, the films were scanned in 75 dpi using an Epson Expression 12000XL photo scanner fitted with a transparency unit. [16]. [c5]Each irradiated strip of film was sampled at its center and deconstructed into its average red, green, and blue (RGB) intensity values. Using least squares regression, an exponential equation is fitted to each color channel resulting in three calibration curves [17]. An example of irradiated film samples and the resulting calibration curves is given in Figure 8. When using EBT3 films, it is important that the calibration and field [c6]set [c7] be from the same batch as the manufacturing process can lead to variations within the blue color channel.

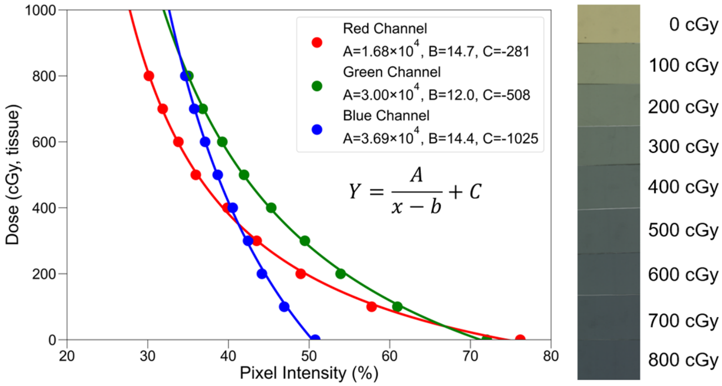

Fig. 8: Calibration curves generated for EBT3 film.

It was [c1]observed that EBT3 films were not sensitive enough to provide high-contrast images using the output of a typical X-ray inspection device. Instead, [c2]radiochromic XRQA2 films offer high image quality at effective dose range of $0.1 - 20$ cGy, [c3]requiring 1% the dose of EBT3. The drawback of [c4]the XRQA2 films is that they are designed for quality assurance and are typically read either through visual inspection or through optical density making it difficult to estimate dose on a per pixel basis [8]. However, these films exhibit a drastic color change when exposed to X-rays, which allows for a study on the feasibility of using a color channel calibration similar to the EBT3 film. Due to the white polyester backing, the XRQA2 films are non-transparent and were

[c5] *MPP*: *Text added.*
[c6] *MPP*: *Text added.*
[c7] *MPP*: ~~use film~~
[c1] *MPP*: ~~found~~
[c2] *MPP*: ~~XRQA2~~
[c3] *MPP*: ~~100 times lower than that~~
[c4] *MPP*: ~~these films is that they are~~

scanned using a reflective unit. The calibration strips were deconstructed into color channels and plotted with dose. Using a general exponential formula, the calibration parameters for each color channel were estimated using a least squares method. The color channel calibration for the XRQA2 film is shown in Figure 9.

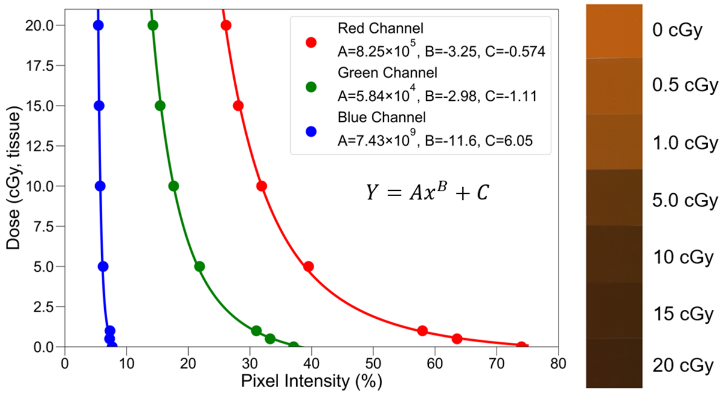

Fig. 9: Calibration curves generated for XRQA2 film.

[c1] [c2]For film measurements, the films were laid flat on the bottom irradiation tray (Shelf1). The PCBA was placed 1 cm above the film using plastic stand-offs to allow the board to sit evenly while irradiated. This arrangement provides a source-to-object distance of 36.1 cm, and a source-to-detector distance of 37.1 cm, giving a magnification of 1.03. The corners of the board were held by an alignment tool which contained steel sheets that act as a guide to allow [c3] the board image to be cropped and aligned properly. [c4]The target dose for EBT3 and XRQA2 film was set at 5 Gy and 5 cGy respectively. The simulation model was updated to include the radiation film, X-ray filters, and the sample tray. Separate inputs were created for the EBT3 and XRQA2 films, as they have distinct layer thicknesses and densities. The film layer thickness, the layer density, and the layer composition are given in Table 2. For each of the film simulations, an input was created for both the simplified and the complex PCBA geometry. Within MCNP, the tally defined was a photon flux grid tally given by the FMESH4 card. This tally was used with a tissue response function to give units of dose for each mesh element within the grid. The tally region only considers the dose within the film's active layer and does not consider the surrounding polyester components. Each mesh element was designed to be 0.038 mm×0.038 mm, which is equivalent to the pixel size given for a 75 dots per inch (dpi) film scan.

[c1] *MPP*: ~~For the film measurement, the edges of the PCBA were attached to 1 cm plastic stand-offs to allow the board to sit evenly while irradiated.~~
[c2] *MPP*: *Text added.*
[c3] *MPP*: ~~for~~
[c4] *MPP*: *Text added.*

Film Type	Layer	Thickness (µm)	Density ($g\,cm^{-3}$)	Composition by Atomic % H	Li	C	N	O	Na	S	Ba	Cl	Al	Bi
EBT3	Transparent Polyester Base	125	1.35	56.8		45.5		18.2						
EBT3	Active Layer	25	1.20	36.4	0.6	27.6		13.3					1.6	
EBT3	Transparent Polyester Base	125	1.35	56.8		45.5		18.2						
XRQA2	Transparent Yellow Polyester	97	1.35	36.4		45.4		18.2						
XRQA2	Adhesive	20	1.20	56.9	0.48	33.2		9.4						
XRQA2	Active Layer	25	1.60	56.2	1.0	27.6	1.6	11.7	22.3			0.1		1.7
XRQA2	White Polyester Base	97	1.60	33.8		42.3		21.6		1.18	1.18			

Table 2: Layer thicknesses and material composition for EBT3 and XRQA2 film.

2.7 Thermoluminescent Dosimetry

To further quantitatively validate the Monte Carlo model, thermoluminescent dosimeters (TLDs) were used. The TLDs used for this experiment were TLD-400s, CaF_2 based dosimeters distributed by ThermoFisher [18]. [c5]These dosimeters are only available as a $3.2\times3.2\times0.89$ mm^3 chip and are designed to share a similar photon response to Si. [c6] [c7]This means that when properly calibrated, these dosimeters can theoretically output a dose in Si directly. By selecting bare regions of the board and regions of high interest, the TLD can act as if it was a pure silicon-based part[c8]. To understand if the calibration to a Si will maintain the same accuracy as a calibration to CaF_2, two separate calibration sets were created for comparison. To determine the dose rate for the TLDs, a simulation model of the TLD calibration procedure within the Rad Source RS1800 was created. This simulation model consists of the aluminum and zinc X-ray filters, an aluminum X-ray sample tray, a 3D printed TLD holder, 30 TLDs, and 0.2032 mm of aluminum [c9]surrounding the TLD holder. The aluminum [c10]was included to ensure charged particle equilibrium [c11][c12] as aluminum [c13]has an atomic number similar [c14]to Si and CaF_2 [19]. For [c15]the CaF_2 and Si TLD simulations, a 130 kV, 1 mA X-ray source was used to achieve a absorbed dose of 1 Gy.

[c1]Three energy deposition tallies within MCNP were [c2]tested to compare accuracy and computational efficiency. For the MCNP transport, the F4, F6, and *F8 energy deposition tallies were considered[c3]. The F4 tally is a volumetric flux tally that, when paired with a photon response function, will output dose in units of Gy. This tally has the advantage of directly outputting absorbed doses in Si, the standard quantity for electronics. This tally is also computationally more efficient than the other two tally types, as electron

[c5] *MPP*: *Text added.*
[c6] *MPP*: ~~CaF_2 shares a similar photon response as Si, meaning that the dosimeters can theoretically be calibrated to output a Si dose directly.~~
[c7] *MPP*: *Text added.*
[c8] *MPP*: ~~on the board~~
[c9] *MPP*: ~~on each side of~~
[c10] *MPP*: ~~acts to give~~
[c11] *MPP*: ~~creating a Bragg-Gray cavity~~
[c12] *MPP*: ~~for the TLDs,~~
[c13] *MPP*: ~~shares a~~
[c14] *MPP*: ~~atomic number~~
[c15] *MPP*: ~~the simulated irradiation,~~
[c1] *MPP*: ~~In the simulated TLD calibration, three~~
[c2] *MPP*: ~~taken into account~~
[c3] *MPP*: ~~for both their accuracy and transport advantages~~

	TLD Dose mGy s^{-1}			
Tally Type	CaF_2, ρ=3.18	CaF_2, ρ=2.32	Si, ρ=2.32	Si, ρ=3.18
F4	7.15	7.32	4.40	4.35
F6	7.12	7.29	4.37	4.32
*F8	7.02	7.16	4.30	4.26

Table 3: Dose rates for CaF_2 and Si TLD calibration using different MCNP transport techniques. All statistical errors were less than 1%.

transport is not considered. The F6 tally is a track length energy deposition tally that will output units of MeV g^{-1}. This tally has the benefit of [c4]producing the part dose rather than a silicon dose which holds more truth to the material compositions used in simulations. When using this tally, electron transport must be considered for small volumes, as electrons are expected to enter and leave the cell boundary. This means that the run time for this tally is approximately twice that of the F4 tally. Last, the *F8 tally is an integrated pulse height tally that outputs units of MeV. This tally is an "energy-in minus energy-out" tally that considers the full electron transport and exhibits the greatest accuracy of the tally types considered. The disadvantage is that this tally requires more particles to be simulated in order to converge on a solution, increasing the run time. Because this tally outputs units of MeV, each result must be divided by the part mass to obtain proper dosimetric units. Absorbed dose rate results for the TLD-400 calibration to CaF_2 and Si are provided in Table 3.

The calibration simulations show that the density makes little difference (≈1%) to the absorbed dose, as the mass of the TLD compensates for energy deposition differences. To keep the TLD calibration as accurate as possible and to conserve the true TLD density, irradiation times were based on the results of the *F8 tally using the CaF_2 density of 3.18 g cm^{-3}. [c1] For all TLD measurements, a Harshaw 5500 utilizing ultra-high purity nitrogen was used [20]. The time-temperature profiles were set to acquire the glow curve using a temperature rate of [c2]25°C s^{-1}, a max temperature of 400°C, and an acquisition time of 23 1/3 seconds. [c3]TLD-400s on average lose 8% of their signal within the first 24 hours after irradiation. To keep fade time consistent, all TLDs were given a 24-hour fade period between irradiation and measurement. After each signal reading the TLDs were annealed in a Nabertherm NA 15/65 HA oven at a temperature of 400°C for one hour before being quenched on a large aluminum block [21].

[c4]TLD-400 calibration sets were created for CaF_2 and Si by calibrating to a dose of 1 Gy in their respective materials. To perform the calibration, an initial irradiation was completed to detect problematic TLDs reading outside

[c4] *MPP*: ~~outputting~~
[c1] *MPP*: ~~The TLD-400 calibration sets were created for CaF_2 and Si by calibrating to a dose of 1 Gy in their respective materials.~~
[c2] *MPP*: ~~25°C~~
[c3] *MPP*: *Text added.*
[c4] *MPP*: *Text added.*

+/- 10% of the mean light readout. Any problematic TLDs were discarded from the calibration set. A second irradiation was performed to calculate each TLD's element correction coefficient (ECC). This factor corrects for discrepancies between individual TLD readouts that occur due to slight inconsistencies in the manufacturing process. A third irradiation calculates the reader calibration factor (RCF). This factor converts the integrated light output measured by the TLD reader into dosimetric units. This factor is unique to each TLD reader, and each TLD type. From the calibration set, the RCF is manually entered into the acquisition settings of a new TLD batch. A field set of dosimeters is then generated by calculating new ECC values using the RCF imported from the calibration set. A field set of dosimeters containing 50 CaF_2-calibrated and 50 Si-calibrated TLDs was created.

On the PCBA, 37 TLD locations were chosen to provide dose estimates in areas with high part density and radiation-sensitive components. For the irradiation, the TLDs were placed in a small 3D printed plastic housing with 0.2032 mm of aluminum on the top and bottom face similar to the calibration procedure. The housings were fastened to the PCBA and irradiated [c1]to a target dose of 1 Gy, similar to the calibration procedure. Each TLD was then carefully removed from its housing and the radiation dose to each TLD was documented. The TLDs were annealed and the board orientation was reversed for a second TLD measurement. For all simulations, the 3D-printed housing and aluminum covers were fully represented in the transport model. Simulations were conducted using the simple and complex models for the PCBA geometries and both board orientations. Images showing the TLD placement on the PCBA and the TLD numbering system are shown in Figure 10. The locations shown give the size of the 3D-printed TLD holder containing the aluminum shielding.

3 Results

3.1 Film Radiography

[c2]For EBT3 and XRQA2 film 1×10^{10} particles were simulated to achieve relative errors less than 10%. This number of simulated particles was based on extrapolated error data from initial runs, as Monte Carlo error reduction follows $1/\sqrt{N}$. The average relative pixel error of the EBT3 and XRQA2 film simulations was 6.7% and 8.6% respectively. For the EBT3 films, the color channel calibration was applied to each pixel of the film measurement [c3]and compared to the simulated results. Dose profiles (Figure 11) show that the Monte Carlo results suffer from noise due to the fine spatial grid. To minimize noise, the per-pixel measurements were averaged over individual components and bare PCBA regions. It was observed that the fluctuations in dose due to attenuating parts correspond well with the transport model and measurement.

[c1] *MPP*: ~~for the same duration used in the calibration procedure~~
[c2] *MPP*: *Text added.*
[c3] *MPP*: ~~scan~~

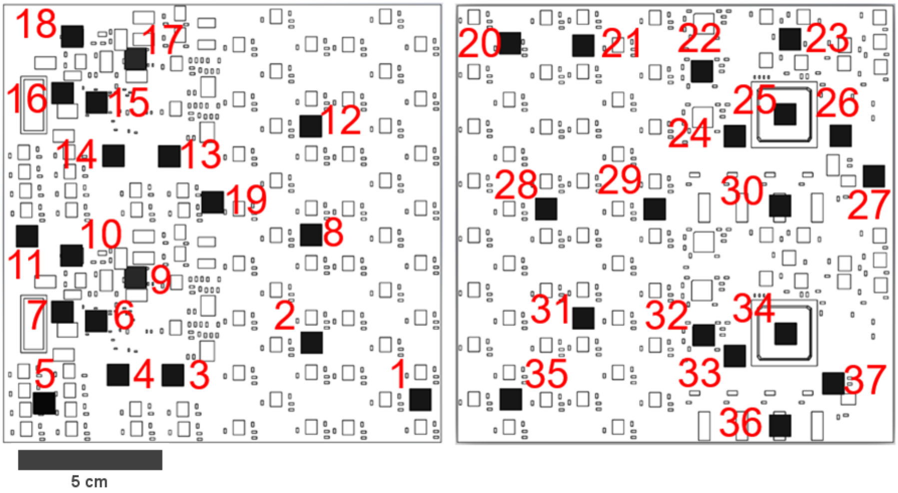

Fig. 10: Numbering system of TLD, and example of MCNP transport geometry for TLD simulation.

Between the components, some small discrepancies were observed which are due to the absence of leads in the simulation model. One key observation is that the measured dose increases in the negative Z-direction even when there are repeating or no structures present. This is thought to be due to the heel effect, where the X-ray intensity increases away from the anode [22]. It is also possible that this is due to the lateral scan artifact, which causes intensity values to vary based on the film location relative to the center of the scanner [7].

The line scan comparisons are given in Figure 12. Comparing the simplified and complex Monte Carlo models, three dose profiles of interest were determined. The first line envelops many parts and was chosen to show the accuracy of the part representation and placement. In this region, the simplified and complex models are nearly identical as the copper distribution throughout this region is fairly consistent. It was also observed that including leads in the simulated material composition leads to larger attenuation over the part regions. For the second line scan, the line passes through the connector pins and BGA, which were changed for the complex model. It was found that the improvements to the connector pins made little difference in the dose profile. For the BGA region, it was found that the complex model improvements made a significant [c1]impact to the accuracy of the dose profile. For the remainder of the scan, the simplified and complex models performed identically. The third line scan was chosen to pass over the highly attenuating tantalum capacitors. For this scan, large differences were observed over the tantalum capacitors, while the rest of the scan remained consistent between the two models. In all of the

[c1] *MPP*: ~~difference in~~

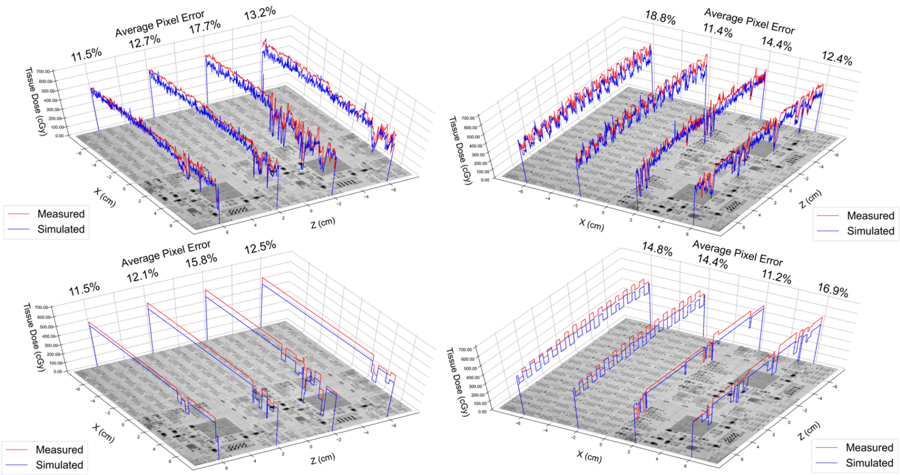

Fig. 11: Dose profile comparisons of simulated and measured EBT3 X-ray films for the complex computational transport model. Per pixel comparison (Top), part averaged comparison (bottom).

scans, the measured data was found to have unpredictable fluctuations directly to the left and right of components due to leads, pads, and overlap.

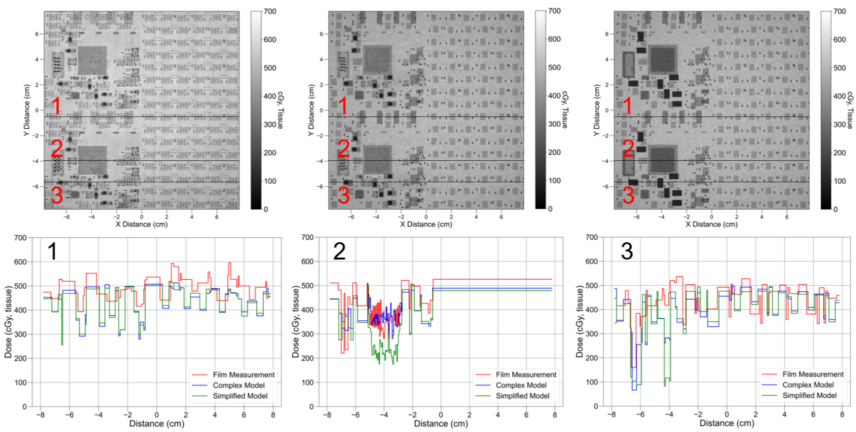

Fig. 12: Part averaged dose profile comparisons between complex and simplified MCNP model.

The comparison of dose profiles for XRQA2 films is shown in Figure 13. [c1]For all XRQA2 film results, the blue color channel was ignored as it showed little variation with dose, and lead to large inconsistencies when included in

[c1] ~~For XRQA2 film~~

the measurement. Across the board, the XRQA2 simulations were shown to overestimate the dose profiles and were found to suffer from a considerable amount of noise. The increase in simulated noise is likely attributed to the difference in density of the active layer when compared to EBT3 film. It is hypothesized that a higher active layer density will lead to a larger variation in the path length of particles as they travel through the film causing noise. If observed closely, it can be seen that these films also suffer from an increase in measured dose in the negative Z-direction.

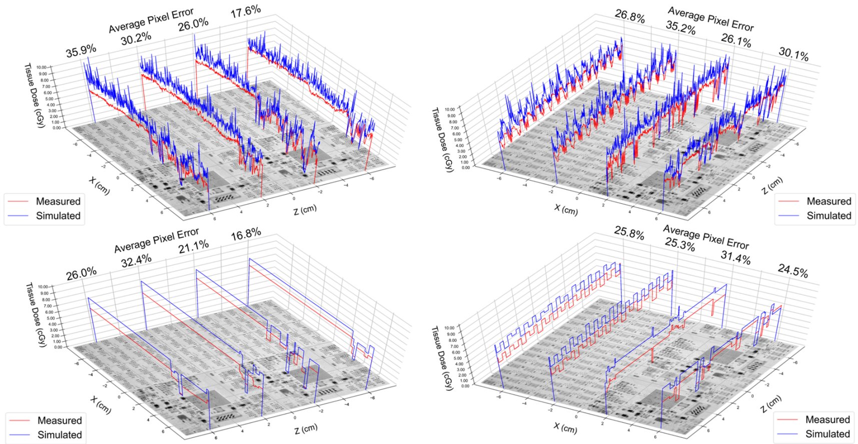

Fig. 13: Dose profile comparisons of simulated and measured XRQA2 X-ray films for the complex computational transport model. Per pixel comparison (Top), part averaged comparison (bottom).

3.2 Thermoluminescent Dosimetry

The TLD results for the CaF_2 calibrated TLDs are shown in Figure 14.[c1] For all TLD simulations, the number of particles simulated was set to 1×10^9 which results in relative errors less than 5%. [c2] Simulations were completed for the F4, F6, and *F8 tallies and compared to measured results. It was found that for the CaF_2 calibration with the BGAs facing towards the source, the simulated dose was consistently higher than the measured dose with the error averaging 5.6%. For the CaF_2 results with the BGA facing away from the source, the results were more evenly distributed with an error of 4.8%. Overall, the profile of the dose matches well with the simulated data except for TLD 26. The difference for TLD 26 is due to a highly attenuating tantalum capacitor that shields the simulated TLD. This could either be from the simulated TLD placement being incorrect from the measurement or may indicate that the representation of the

[c1] *MPP*: *Text added.*
[c2] *MPP*: ~~For the TLDs,~~

tantalum capacitors was slightly inaccurate. However, this behavior was not observed for TLDs 7 or 9, which are surrounded by four tantalum capacitors, and was only slightly observable in TLD 37 which sits directly on top of a tantalum capacitor.

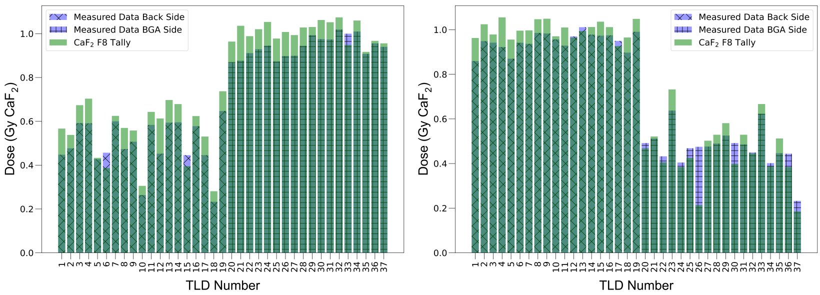

(a) CaF_2 tally results with BGA facing the source.

(b) CaF_2 tally results with BGA facing away from the source.

Fig. 14: MCNP *F8 tally results compared with CaF_2 calibrated TLDs.

The TLD results for Si calibration are shown in Figure 15. The Si TLD calibration showed a slight improvement compared to the CaF_2 calibration with the average error for the BGA facing the source being 4.7% and the error for the BGA facing away from the source being 4.7%. Once again, the error for TLD 26 persists, indicating that there is a discrepancy in the transport model. For the TLDs calibrated to Si, it was observed that Si-based components on the board followed the same trend as the TLDs, with components facing the source receiving 0.86-1.15 Gy and components on the back of the board receiving 0.55-0.75 Gy. This provides evidence that TLD-400s are accurate at representing component dose and could be used in place of or near a component to provide radiation dose estimates. For both the CaF_2 and Si calibrations, the F4 and F6 simulation data were observed to have slightly higher errors between 5-7% when compared with the measured data.

4 Conclusions

BGAs require X-ray inspection to confirm a proper connection between the electronic package and the PCBA. During the inspection, the PCBA is exposed to ionizing radiation that, over time, could affect the performance of radiation-sensitive components. Monte Carlo methods can be used to provide dose estimates, but the conversion process between PCBA design software to radiation model geometry typically removes significant details such as leads, solder, traces, and internal structures. To confirm the significance of these details, and to confirm that the model still remains accurate for radiation dose estimates, a validation study was performed using film and TLD measurement. To

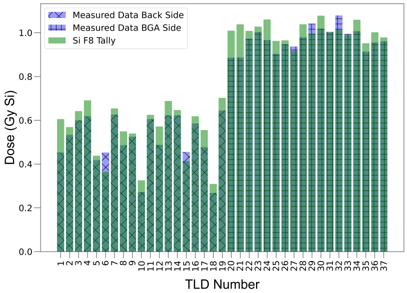

(a) Si tally results with BGA facing the source.

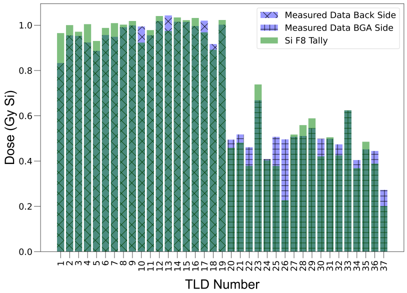

(b) Si tally results with BGA facing away from the source

Fig. 15: MCNP *F8 tally results compared with Si calibrated TLDs.

create the Monte Carlo model, a test PCBA was designed and manufactured by KSU-EDL. Using exported files from the PCBA design software ULTIboard, a simple CAD model was created. X-ray films were used to identify improvements to the model, and a second detailed PCBA model was created.

Monte Carlo simulations were performed on the simplified and complex transport models. For the EBT3 films, the dose profiles from the Monte Carlo simulation matched the film measurement between 13-24% for individual line scans. For the XRQA2 films, errors fitting a calibration function to the blue color channel caused an overestimation of the dose profiles across the board. When comparing the dose profiles of the simplified and complex transport models, key differences were observed in the representation of solder balls for the BGA and the internal representation of the tantalum capacitors. For the TLD simulations, the measured and simulated CaF_2 TLD results were found to be within 5.6%. For TLDs calibrated to a Si dose, the error was reduced to 4.7%. For both TLD simulations, substantial differences were observed on TLD 26, providing evidence of a model discrepancy. From this study, it was concluded that copper traces may be homogenized throughout the board material with minimal effects on the dose rates to parts. It was also found that the representation of solder balls on BGAs and highly attenuating internal structures, such as those in capacitors, are large contributors to the accuracy of radiation dose estimates.

In the future, this work should be expanded to include correction for the radiation heel effect observed in the film dosimetry results. A study should also be performed to determine if the accuracy of the [c1]film simulations may be [c2]improved using a photon response function of the active layer material rather than a tissue response. [c3]Using the dose profiles of the EBT3 film,

[c1] *MPP*: ~~films~~
[c2] *MPP*: ~~increased~~
[c3] *MPP*: ~~A study could also be performed to determine density corrections for materials based on film results.~~

density corrections to components could be applied to improve part representation. This study will then need to undergo an iteration process with TLDs to ensure the density improvements are accurate. For the TLDs, the study should be expanded to determine the parameters and conditions for which a Si calibration may be used to accurately determine component dose. If performed properly, a database of components that conform to a silicon dose standard may be cataloged and used to improve the radiation hardening of electronic assemblies.

5 Declarations

5.1 Ethics approval and consent to participate

Not applicable

5.2 Consent for publication

Informed consent was obtained from all individual participants included in the study.

5.3 Availability of data and material

Not applicable

5.4 Competing Interests

The authors declare that they have no competing interests.

5.5 Funding

This work was funded by the Department of Energy's Kansas City National Security Campus, operated by Honeywell Federal Manufacturing & Technologies, LLC under contract number DE-NA0002839.

The computing for this project was performed on the Beocat Research Cluster at Kansas State University, which is funded in part by NSF grants CNS-1006860, EPS-1006860, EPS-0919443, ACI-1440548, CHE-1726332, and NIH P20GM113109.

5.6 Authors' contributions

Michael P. Pfeifer - Methodology, Software, Validation, Data curation, Writing – original draft.

Nathanael Simerl – Software, Data curation, Writing – review & editing.

John Porter – Funding acquisition.

Walter J. McNeil – Supervision, Writing – review & editing.

Amir A. Bahadori – Conceptualization, Supervision,
Writing – review & editing.

5.7 Acknowledgements

The authors would like to thank the Nuclear Regulatory Commission Fellowship program for additional support.

References

[1] LGA PGA BGA: What's the Difference Between the Grid Arrays? https://www.raypcb.com/lga-pga-bga/ (2021)

[2] Wickham, M., Hunt, C., Adams, D.M., Dunn, B.D.: An investigation into ball grid array inspection techniques. Technical report, European Space Agency (1999)

[3] Bernard, D., Lane, R., Blish, R.: Considerations for minimizing radiation doses to components during x-ray inspection. Technical report, Buckinghamshire (2022)

[4] Campola, M., O'Bryan, M.: Overview of the Radiation Effects & Analysis Group and Space Radiation Physics Office. https://radhome.gsfc.nasa.gov/radhome/RadDataBase/RadDataBase.html (2021)

[5] Pfeifer, M., Simerl, N., Strahler, R., Casburn, J., Dodson, M., Porter, J., McNeil, W., Bahadori, A.: Validation of Radiation Transport Methods for Ball Grid Array Inspection Systems. https://www.ans.org/pubs/transactions/article-48319/ (2020)

[6] NI Ultiboard. National Instruments

[7] GAFCHROMIC™ DOSIMETRY MEDIA, TYPE EBT-3. http://www.gafchromic.com/documents/EBT3_Specifications.pdf

[8] Gafchromic XR film. http://www.gafchromic.com/documents/PC-11805_Gafchromic_XR. (2016)

[9] SolidWorks. Dassault Systems, Vélizy-Villacoublay, France (2017)

[10] TransMagic. TransMagic, Westminster, CO

[11] Cell Research Irradiator - Rad Source Technologies. https://www.radsource.com/cell-research/

[12] Goorley, T., James, M., Booth, T., Brown, F., Bull, J., Cox, L., Durkee, J., Elson, J., Fensin, M., Forster, R., *et al.*: Initial mcnp6 release overview. Nuclear Technology **180**(3), 298–315 (2012)

[13] Martz, R.: The MCNP6 Book On Unstructured Mesh Geometry: User's Guide For MCNP 6.2. https://mcnp.lanl.gov/pdf_files/la-ur-17-22442.pdf (2017)

[14] Poludniowski, G., Landry, G., DeBlois, F., Evans, P., Verhaegen, F.: Spekcalc: a program to calculate photon spectra from tungsten anode x-ray tubes. Physics in Medicine & Biology **54**(19), 433

[15] Pfeifer, M., Simerl, N., Strahler, R., Casburn, J., Porter, J., McNeil, W., Bahadori, A.: Methods for estimating x-ray machine output through measurement and simulation. Applied Radiation and Isotopes (2022)

[16] Epson Expression 12000XL Photo Scanner. https://epson.com/For-Work/Scanners/Photo-and-Graphics/Epson-Expression-12000XL-Photo-Scanner/p/12000XL-PH (2023)

[17] Efficient Protocols for Accurate Radiochromic Film Calibration and Dosimetry. http://www.gafchromic.com/documents/Efficient Protocols for Calibration and Dosimetry.pdf

[18] TLD-400™ Thermoluminescent Dosimetry Material. https://www.thermofisher.com/order/catalog/product/SNO48835

[19] Kerris, K.: The aurora dosimetry system. Technical report (1976)

[20] Harshaw TLD Model 5500 Readers. https://www.thermofisher.com/order/catalog/pr

[21] Ovens up to 300 °C, also with Safety Technology According to EN 1539 Nabertherm. https://nabertherm.com/en/products/laboratory/ovens-and-forced-convection/ovens-300-degc-also-safety-technology-according-en

[22] Murphy, A., Shetty, A.: Anode heel effect Radiology Reference Article Radiopaedia.org. https://radiopaedia.org/articles/anode-heel-effect